Melting behavior of SiO2 up to 120 GPa

Denis Andrault, G. Morard, G. Garbarino, M. Mezouar, Mohamed Ali Bouhifd, T. Kawamoto

Melting behavior of SiO_2 up to 120 GPa

D. Andrault[1,*], G. Morard[2], G. Garbarino[3], M. Mezouar[3], M.A. Bouhifd[1], T. Kawamoto[4]

[1] Université Clermont Auvergne, CNRS, IRD, OPGC, LMV, Clermont-Ferrand, France.

[2] Sorbonne Université, MNHN, CNRS, IRD, IMPMC, Paris, France.

[3] European Synchrotron Radiation Facility, ESRF, Grenoble, France.

[4] Department of Geoscience, Faculty of Science, Shizuoka University, Shizuoka, Japan.

* Corresponding Author: denis.andrault@uca.fr; Tel: 00334 7334 6781

ABSTRACT

The structure of liquid silicates is commonly described as a statistical mixture of various atomic entities with relative abundances that can vary with pressure, temperature and composition. Unfortunately, this view remains largely theoretical due to scarce experimental reports on the silicate melt structure, in particular under pressure. We performed X-ray diffraction of the SiO_2 end-member to probe the melting curve up to ~120 GPa and 7000 K, and the melt structure up to ~80 GPa. We confirm the steep increase of the melting curve above ~14 GPa when stishovite becomes stable over coesite in subsolidus conditions, with a slope of about 80 K/GPa. Then, around 45 GPa and 5400 K, the melting curve flattens significantly, an effect most likely reflecting the densification of the SiO_2 melt structure. The signal of diffuse X-ray scattering is compatible with a change of the Si coordination number from 4 to 6 along the melting curve, in agreement with previous works reporting a similar evolution during the cold compression of SiO_2-glass. Because of the limited pressure range (within 10 to 20 GPa) in which the melting curve changes its slope, we speculate a difficult coexistence of tetrahedral SiO_4 and octahedral SiO_6 units in SiO_2 melt at high pressures.

KEYWORDS

SiO_2-silica, melting diagram, melt structure, lower mantle pressures

ACKNOWLEDGEMENTS

We thank anonymous reviewers for helpful comments. This research was financed by the French Government Laboratory of Excellence initiative n°ANR-10-LABX-0006, the Région Auvergne and the European Regional Development Fund. This is Laboratory of Excellence ClerVolc contribution N°XX.

I. INTRODUCTION

Although SiO_2 is rarely present as a pure phase in mantle rocks, it is a dominant component of terrestrial planets. Because SiO_2 is highly refractory, its melting curve significantly affects the melting diagram of silicates present in the crust and the mantle. At subsolidus conditions, SiO_2 undergoes a major transition from coesite to stishovite, at a pressure of ~14 GPa for a temperature of 3000 K (Zhang et al. 1993). The transition involves a change of the Si coordination number from tetrahedral "SiO_4" to octahedral "SiO_6" units, accompanied with a density change of ~30% (Akaogi et al. 2011). This transition occurs in all silicates with a transition pressure that depends on composition. The structural changes are major and induce a divergence of physical and chemical properties between the shallower and deeper parts of planetary mantles.

The change of the Si coordination number is also expected to occur in silicate melts (Sanloup et al. 2013). For SiO_2, the experimental investigation on the melt is strongly hampered by a steep increase of the melting curve at pressures higher than the coesite to stishovite transition: The melting temperature was reported to increase from 3000 to 3900 K between ~14 GPa and ~22 GPa (Shen and Lazor 1995). Such a steep Clapeyron slope ($dT/dP=\Delta V/\Delta S$) denotes a large volume of fusion between stishovite and a low density melt (LDM) containing Si in 4-fold coordination. In contrast, the Clapeyron slope of the melting curve is almost flat below ~14 GPa, which implies a negligible density contrast between coesite and LDM (Zhang et al. 1993). The brutal change of slope of the melting curve at ~14 GPa shows that LDM is maintained at pressures above the Si coordination change in the solid state.

The pressure-induced Si coordination change in amorphous SiO_2 was investigated experimentally at room temperature (Benmore et al. 2010; Lin et al. 2007; Murakami and Bass 2010; Sato and Funamori 2010) and theoretically (Meade et al. 1992; Stixrude and Karki 2005; Takada et al. 2016; Usui and Tsuchiya 2010). In both cases, the transformation to an octahedral-based SiO_2 structure is clearly demonstrated. At high temperatures, the formation of a high-density melt (HDM), with a similar structure to the high-density glass potentially, would induce a smaller density contrast between stishovite and HDM, compared to stishovite and LDM. This would induce the flattening of the Clapeyron slope of the melting curve with increasing pressure. This line of reasoning agrees with the report of a moderate increase of the melting temperature from 5000 K to 5800 K with increasing pressure from 40 to 120 GPa (Usui and Tsuchiya 2010). Still, large inconsistencies remain. For example, the melting temperature was reported from 4400 K (Luo et al. 2002) to 5250 K (Usui and Tsuchiya 2010) at a pressures around 50 GPa. In addition, neither the change in Clapeyron slope of the SiO_2 melting curve at increasing pressure, nor the change in Si coordination number in the melt have been properly documented.

II. MATERIALS AND METHODS

2.1 Experimental design

We first refined the melting curve of SiO_2 up to ~120 GPa using the laser-heated diamond anvil cell (LH-DAC) coupled with *in situ* X-ray diffraction. Samples consisted of small shards of pure SiO_2 glass, typically of 20-50 µm across and 10-15 µm thick. The glass was loaded in the pressure chamber between two KCl layers of similar thickness. The use of a KCl makes the X-ray analysis more difficult, due to intense KCl peaks; however, a critical advantage is to minimize the axial thermal gradients within the sample. In addition, soft KCl layers favor homogenous sample pressure at high temperature. The amount of water trapped in the pressure chamber was minimized by performing all sample-loading operations under N_2-flux in a glove bag. Samples were heated alternatively using a CO_2 laser on one side or two fiber-lasers on both sides of the DAC. We found that SiO_2 absorbs relatively well the 1 µm radiation of fiber-lasers after the sample is already heated to high temperatures using the CO_2. In all cases, laser spots were more than 20 µm in diameter.

In a second series of experiments, we probed the structure of SiO_2 melt at high pressures. We did not use a pressure medium in this case to prevent artifacts that could arise from its diffuse scattering, if the pressure medium eventually melts. Yet, a small grain of KCl was loaded in the gasket hole for the measurement of the nominal pressure. The sample geometry consisted in two thin disks of SiO_2 quartz single crystal in direct contact with the diamonds, between which a little bit of Si-metal powder was distributed. The role of Si-metal is to couple with fiber-lasers in order to initiate the sample heating before the annealed SiO_2 could eventually absorb the laser radiation by itself. We preferred the addition of Si to Pt powder that would have also provided an internal pressure calibrant, because Pt melts at lower temperature than SiO_2 at high pressures; its signal of diffuse scattering would have hampered the study of SiO_2-melt. The presence of a minor excess of Si in SiO_2 melt should not affect significantly the melt structure, nor the mechanism of the pressure-induced Si coordination change. Upon laser heating, SiO_2 eventually melts at mid-distance between the two diamond culets. Then, further increase of the laser power induces a thicker layer of molten SiO_2. In such a sample experiencing large axial temperature gradient, some SiO_2 always remain solid at the contact with cold diamonds. More importantly, the temperature gradient within the molten part of the sample should be minor, due to turbulent convection in the high-pressure melt.

2.2 Determination of pressure and temperature in the laser heated diamond anvil cell

We used the equation of state of KCl (Dewaele et al. 2012) to determine the nominal pressure at 300K before and after laser heating. Then, the sample pressure at high temperature was determined using two different cross-calibrated methods: (i) the P-V-T equation of state of stishovite (Wang et al. 2012) and (ii) the nominal pressure corrected by $X_{Th}\alpha KT$ to account for the increase of pressure in the laser spot (X_{Th} is an adjustable parameter, α and K are thermal expansion and bulk modulus, respectively, of coesite (Akaogi et al. 2011) at nominal pressures below 14 GPa and stishovite (Wang et al. 2012) for pressures above). We used samples loaded in KCl and heated below the melting curve

to calibrate the value of X_{Th}. For this sample geometry, the two methods give pressures within +/- 5 GPa for X_{Th} values increasing linearly from 35% to 90%, when temperature is increased from 4000 to 7000 K, respectively. At the melting temperature, the second method is preferred, because the remaining fraction of stishovite grains may encounter a temperature lower than the SiO_2-melt, because they are located closer to the diamonds. The second method was also used to determine the pressure for DAC loadings without KCl pressure medium.

Temperatures up to 7000 K were determined based on spectroradiometric measurements (Fig. 1). To make these measurements accurate, a critical parameter of the optical set-up is the use of reflective Schwarzfield-type telescopes and the absence of any refractive device along the optical path, in order to prevent chromatic aberration (Schultz et al. 2005). Temperature measurements are performed with a precision of ±100 K and a reproducibility better than ±30 K. When not using KCl insulating layers in the DAC, the temperature uncertainty could be twice larger, due to steeper axial temperature gradient. We note that the measured temperature corresponds to the hottest part of the sample, where thermal emission is the most intense.

The sample behavior was monitored *in situ* using an X-ray beam much smaller than the hot-spot on the sample (see below). The fluorescence (in the visible range of wavelength) of the irradiated KCl pressure medium, or irradiated Re-gasket, was used to adjust the spectrometer position, in order to perform the temperature measurement at the position of the X-ray beam. The spectrometer alignments were carefully checked before and after each melting experiments.

2.3 X-ray diffraction measurements

At the ID27 beamline of the ESRF (Grenoble, France), we used a monochromatic X-ray beam of 0.3738 Å wavelength focused by two Kirkpatrick-Baez mirrors onto a spot of less than 2x2 μm^2. Diffraction patterns were recorded using a MAR-160 CCD detector and integrated using DIOPTAS (Prescher and Prakapenka 2015). Acquisition times extended to 10 sec and 300 sec for solid and molten SiO_2 samples, respectively. For experiments dedicated to the determination of the melting curve, volumes and relative abundances of SiO_2 and KCl were refined using the XRDUA code (De Nolf et al. 2014). For experiments dedicated to probe the structure of SiO_2-melt, we inserted Soller slits between the DAC and the CCD detector. These slits filter out a major fraction of the Compton diffusion coming from diamonds (Weck et al. 2013), which results in a significant improvement of the signal of X-ray diffuse scattering coming from the melt. We first recorded the X-ray diffuse scattering of SiO_2 glass under compression up to ~50 GPa, before we performed measurements at high temperatures in SiO_2 melt up to 80 GPa. In both cases, we also recorded the diffuse background coming from diamond anvils (Compton diffusion). For the melt, small diffraction peaks of not-molten stishovite were eventually visible in the Q region between 1 and 8 $Å^{-1}$. The peaks were carefully fitted by Gaussian functions and subtracted. Then, after subtraction of the diamond Compton diffusion, the scattering signal coming from the sample was normalized to obtain the scattering factor S(Q). Finally,

the wavelength position of the first sharp diffraction peak (FSDP) was extracted from the S(Q) using a Gaussian function coupled with a polynomial background.

III. RESULTS AND DISCUSSION

3.1 A steep SiO_2 melting curve up to 45 GPa

We first refine the melting curve of SiO_2 up to ~120 GPa using the LH-DAC coupled with *in situ* X-ray diffraction. With increasing temperature, the glass starting material first crystallizes in coesite below 14 GPa, stishovite or in the $CaCl_2$-form above ~60 GPa (Andrault et al. 1998). The presence of thin and continuous diffraction rings are evidences for fine crystalline SiO_2 powders under a moderate temperature gradient within the X-ray beam (Fig. 2A). At a sample temperature interpreted hereafter as the melting point of SiO_2, several changes occur simultaneously (such as reported in (Andrault et al. 2014)): (i) Additional increase of the laser power does not induce an increase of the sample temperature (discussed in (Geballe and Jeanloz 2012)); (ii) texture of diffraction rings becomes spottier; (iii) position of diffraction spots on the image plate changes rapidly at constant temperature; (iv) integrated intensity of the SiO_2 diffraction peaks decreases severely relative to the KCl pressure medium (Fig. 2); (v) upon quenching, intense stishovite peaks reappear, which certifies the presence of non-crystalline (i.e. molten) SiO_2 within the X-ray spot at high temperature. The reason why all diffraction peaks of SiO_2 do not disappear abruptly at the melting temperature is the unavoidable axial temperature gradient between the two diamonds. Also, the SiO_2 melt may absorb the laser radiation less than solid SiO_2, resulting in a relatively lower heating efficiency when the sample is partially molten. This can explain the temperature plateau despite an increase of the laser power.

Our measurements confirm the steep increase of the SiO_2 melting temperature above ~14 GPa (Fig. 3, Table 1), in agreement with previous experimental (Shen and Lazor 1995) and theoretical (Belonoshko and Dubrovinsky 1995; Usui and Tsuchiya 2010) studies. Within experimental uncertainties, the melting curve appears linear between ~15 and ~45 GPa. The Clapeyron slope of ~80 K/GPa remains ~4 times smaller than that reported at ~300 K/GPa for the coesite to stishovite transition (Akaogi et al. 2011). Basic thermodynamic relations apply around the triple point where coesite, stishovite and the LDM of SiO_2 coexist (Table 2). As a consequence, we estimate the volume of fusion of stishovite ($2x\Delta V_{Melting}/(V_{LDM}+V_{Sti})$) at ~28% from the combination of the volume change of ~28% at the subsolidus transition (Akaogi et al. 2011) and a negligible volume of fusion of coesite derived from the quasi-horizontal melting line between 9 to 14 GPa (Zhang et al. 1993). On the other hand, the entropy of melting of stishovite (ΔSm) is estimated to ~60 J/molK, a value 4 times larger than the entropy change at the coesite-stishovite transition (Akaogi et al. 2011).

3.2 A relatively flat SiO_2 melting curve from 45 to 90 GPa

The response of our samples to laser heating was different below and above a pressure of ~45 GPa. Between ~15 and ~45 GPa, after the onset of sample melting between ~3000 and ~5400 K (Fig. 3), further increase of the laser power always yield to the same pressure-temperature conditions of ~45 GPa and ~5400 K. This behavior could result from the very large volume of fusion (~28%, see above). Increasing the amount of melt by LH within a nearly constant sample volume in the DAC would logically result in a significant increase of the sample pressure. Above ~45 GPa, this effect is not observed anymore; full sample melting could be achieved within the X-ray spot at each given experimental pressure.

Between ~45 to ~90 GPa, the SiO_2 melting curve presents a Clapeyron slope of ~13 K/GPa, which is ~6 times lower than that observed at lower pressures (Fig. 3). The difference cannot result from subsolidus properties, because the stability field of stishovite extends continuously between ~15 and ~90 GPa below the melting line. Instead, it can be related to the evolution of the structure of the SiO_2 melt. A smaller Clapeyron slope (dT/dP) above 45 GPa denotes either a smaller volume of fusion (ΔVm) and/or a higher entropy of fusion (ΔSm). A higher ΔSm above 45 GPa is improbable, because we expect large structural similarities between stishovite and HDM, as they both contain most of the Si in a 6-fold coordination (Benmore et al. 2010; Lin et al. 2007; Meade et al. 1992; San et al. 2016; Sato and Funamori 2010). Instead, their structural similarities suggest a lower ΔSm. Therefore, the flattening of the melting slope above ~45 GPa is likely to result from a decrease of the volume of fusion due to the presence of a HDM of SiO_2 above the melting curve.

Now, if we consider a fictive triple point between LDM, HDM and stishovite at ~45 GPa and 5400 K, we can use Clapeyron relations ($\Sigma\Delta V=0$, $\Sigma\Delta S=0$ around triple points, and $dT/dP=\Delta V/\Delta S$) to retrieve the thermodynamical parameters of these three phases. Assuming a negligible entropy difference between LDM and HDM ($\Delta S_{LDM\text{-}HDM}$), the stishovite volume of fusion (ΔVm) is estimated to ~5.3% above ~45 GPa (see details of the calculation below Table 2). ΔVm becomes 6.6 % or 4.0 % for hypothetical $\Delta S_{LDM\text{-}HDM}$ values of e.g. -15 or 15 J/mol.K, respectively. Such range of ΔVm values is comparable to the density contrast (reported at ~3 %) between stishovite and a glass compressed above 45 GPa at room temperature (Petitgirard et al. 2017). Then, we can estimate a volume difference of ~25% between LDM and HDM melts. This value is marginally affected (+/- 2%) by changing $\Delta S_{LDM\text{-}HDM}$ in a range of possible values. Such volume change is comparable to the 28% reported between coesite and stishovite (Akaogi et al. 2011). We finally estimate the SiO_2 LDM and HDM densities at ~3.26 10^3 and ~4.17 10^3 kg/m^3, respectively, at 45 GPa and 5400 K (Table 2). Such LDM density is consistent with a previous theoretical report considering less than 10% Si in 6-fold coordination in the melt (Takada et al. 2016).

3.3 Melting of the $CaCl_2$-form of SiO_2 above 90 GPa

Above ~90 GPa, the slope of the SiO_2 melting curve increases slightly to ~35 K/GPa to yield a melting temperature of ~7000 K at ~120 GPa. The progressive increase of the Clapeyron slope could be related to the 2nd order phase transformation from stishovite to the $CaCl_2$-type polymorph (Fig. 3), even though the location of this phase boundary in the P-T diagram remains controversial (see (Fischer et al. 2018) and references therein). In fact, our X-ray measurements confirm that the subsolidus phase transformation occurs between ~80 and ~100 GPa at ~5400 K (Fig. 4). The change of slope of the melting curve is unlikely to come from a difference of volume between the two SiO_2 polymorphs, because it was reported to be insignificant up to ~120 GPa, at least at 300 K (Andrault et al. 2003). In contrast, the higher entropy of the $CaCl_2$-form, compared to stishovite, implies a lower entropy of melting (ΔSm) above the transition pressure and, consequently, a steeper melting curve (because $dT/dP=\Delta Vm/\Delta Sm$). In addition, the strain energy becomes significant with increasing pressure above the transition. The $CaCl_2$ distortion of the stishovite-based lattice observed at ~107 GPa and 5400 K corresponds to a strain energy of ~2 kJ/mole (Andrault et al. 2003). This value is significant compared to the enthalpy of fusion of quartz of 9.4 kJ/mole (Akaogi et al. 2011). Thus, the stabilization energy associated to the $CaCl_2$-distortion can modify the Clapeyron slope of the melting curve.

3.4 Comparison with previous works

Previous LH-DAC experiments suggested an even steeper Clapeyron slope than ours above ~14 GPa (Shen and Lazor 1995). However, after correction of the nominal pressures of the early experiments regarding the pressure increase due to laser heating in the DAC, the two data sets are in fact quite similar to each other. On the other hand, our melting curve plot in relatively good agreement with theoretical calculations, except in a few aspects (Fig. 3). The experimental melting slope remains steep, with little pressure-induced flattening, up to pressures higher than reported in theoretical studies (Belonoshko and Dubrovinsky 1995; Luo et al. 2002; Usui and Tsuchiya 2010). When it eventually flattens around 45 GPa and up to 90 GPa, the SiO_2 experimental melting curve is found parallel, but at 200-300 K higher temperatures, compared to the most recent calculation (Usui and Tsuchiya 2010). The significant increase of melting temperature observed experimentally above ~90 GPa is not reported in any theoretical studies yet.

We note an important discrepancy, of e.g. ~1000K for the melting temperature at 45 GPa, among the previous theoretical studies (Belonoshko and Dubrovinsky 1995; Luo et al. 2002; Usui and Tsuchiya 2010). It could come from the difficulty to model properly the local structure in SiO_2 melt, in particular the strength of the Si-based structural units in LDM and HDM, respectively. Then, compared to shock compressions, our measurements plot at the upper limit of the Hugoniot plots of (solid) quartz and fused quartz (see (Akins and Ahrens 2002) and references therein). Using this technique, one generally identifies the melting temperature when melting is truly achieved at higher impact energies, rather than in the solid at the highest temperatures, before the solid melts. However, this remains a matter of interpretation and the range of temperature uncertainties is large.

3.5 Analysis of the SiO_2-melt structure factors

Polyamorphism in liquid SiO_2 has been extensively discussed in the past by theoretical approaches (e.g. (Brazhkin et al. 2011; Lin et al. 2007; San et al. 2016; Takada et al. 2016)). To address experimentally the structural evolution of liquid SiO_2 under high pressures, we performed LH-DAC experiments coupled with the Soller slits system installed at the ID27 beamline (Weck et al. 2013). This maximizes the signal of the SiO_2 melt over the noise from the sample environment. No KCl pressure medium was used for these experiments. First, we collected diffraction patterns for the cold-compression of SiO_2 glass up to ~45 GPa, in order to validate our experimental measurements of the structure factors S(Q). Our results are found in good agreement with previous studies (e.g. (Prescher et al. 2017)). Spectra present a first sharp diffraction peak (FSDP) around 2 $Å^{-1}$, a second, less intense, around 5 $Å^{-1}$ and a new contribution growing with increasing the pressure between 3 and 3.5 $Å^{-1}$ (Fig. 5). These experimental features have been correlated to the gradual compaction of the structure of amorphous SiO_2 (Benmore et al. 2010; Prescher et al. 2017; Sato and Funamori 2010).

We then recorded diffuse patterns of SiO_2 melt between ~25 and ~75 GPa, which we normalized to obtain S(Q) (Fig. 6). In comparison to the glass, the same FSDP position is found at higher pressure in the melt (Figs. 7 and 8). In addition, the new diffraction peak starts growing between 40 and 54 GPa, and 18.5 and 30.5 GPa, for the melt and the glass, respectively (Fig. 5). In the melt, the shift of the FSDP occurs prior to the appearance of the new diffraction peak, a similar behavior as in the glass (Benmore et al. 2010; Prescher et al. 2017; Sato and Funamori 2010). This effect has been associated to the first regime of the compression where the structural changes are dominated by the compaction of the oxygen network (Wu et al. 2012), before Si changes its coordination number at higher pressures. At pressures higher than ~54 GPa, the additional contribution between 3 and 3.5 $Å^{-1}$ appears clearly in the signal of SiO_2-melt diffuse scattering. At this point, the position of the FSDP is found above 2.2 $Å^{-1}$ and, at 76 GPa, the melt presents the same FSDP position as the glass at ~45 GPa (Fig. 8). All experimental features are similar to those observed in the glass upon change of Si coordination number from 4 to 6 (Benmore et al. 2010; Inamura et al. 2004; Meade et al. 1992; Prescher et al. 2017; Sato and Funamori 2010).

It appears clear that the structural changes occur at higher pressures in the liquid than in the glass. Regarding the extremely high temperatures considered (between 5250 K and 6200 K, Fig. 6), this could be an effect of thermal pressure; the sequence of structural compaction may take place for similar SiO_2 volumes in the glass and in the melt. However, higher temperature requires higher pressure to achieve a similar SiO_2 volume. This hypothesis is supported by the large similarities between diffraction patterns recorded in the liquid and in the glass.

IV. CONCLUSION

The compaction mechanisms of liquid and amorphous SiO_2 are complex and involve various atomic processes. Our experimental measurements suggest a change of the SiO_2 melt structure in a relatively narrow range of pressures, within 10-20 GPa, around 45 GPa. Such evolution is compatible with a previous work investigating the Si coordination change from 4 to 6, e.g. in a SiO_2-glass using transverse acoustic wave velocities (Murakami and Bass 2010). In our experiments, the change in the SiO_2 melt structure is recognized based on (i) a change in the Clapeyron slope of the SiO_2 melting curve and (ii) the occurrence of the new diffraction peak between 3 and 3.5 $Å^{-1}$. The relative sharpness of the structure change in the melt suggests a dominant role of the covalent character of Si-O bonds in the melt (Lin et al. 2007), which could induce a significant difference in energy between the tetrahedral "SiO_4" and octahedal "SiO_6" electronic configurations as a function of pressure and temperature. The two different melt structures could be relatively incompatible with each other, in agreement with previous reports (Brazhkin et al. 2011; Lin et al. 2007; Takada et al. 2016)).

REFERENCES

Akaogi M, Oohata M, Kojitani H, Kawaji H (2011) Thermodynamic properties of stishovite by low-temperature heat capacity measurements and the coesite-stishovite transition boundary Am Miner 96:1325-1330

Akins JA, Ahrens TJ (2002) Dynamic compression of SiO_2: A new interpretation Geophys Res Lett 29:1394

Andrault D, Angel RJ, Mosenfelder JL, Le Bihan T (2003) Equation of state of stishovite to lower mantle pressures Am Miner 88:301-307

Andrault D, Fiquet G, Guyot F, Hanfland M (1998) Pressure-induced landau-type transition in stishovite. Science 23:720-724

Andrault D, Pesce G, Bouhifd MA, Bolfan-Casanova N, Henot JM, Mezouar M (2014) Melting of subducted basalt at the core-mantle boundary Science 344:892-895

Belonoshko AB, Dubrovinsky LS (1995) Molecular-dynamics of stishovite melting Geochim Cosmochim Acta 59:1883-1889

Benmore CJ, Soignard E, Amin SA, Guthrie M, Shastri SD, Lee PL, Yarger JL (2010) Structural and topological changes in silica glass at pressure Phys Rev B 81

Brazhkin VV, Lyapin AG, Trachenko K (2011) Atomistic modeling of multiple amorphous-amorphous transitions in SiO2 and GeO2 glasses at megabar pressures Phys Rev B 83

De Nolf W, Vanmeert F, Janssens K (2014) XRDUA: crystalline phase distribution maps by two-dimensional scanning and tomographic (micro) X-ray powder diffraction Journal of Applied Crystallography 47:1107-1117 doi:doi:10.1107/S1600576714008218

Dewaele A, Belonoshko AB, Garbarino G, Occelli F, Bouvier P, Hanfland M, Mezouar M (2012) High-pressure high-temperature equation of state of KCl and KBr Phys Rev B 85 doi:10.1103/PhysRevB.85.214105

Fischer RA et al. (2018) Equations of state and phase boundary for stishovite and CaCl2-type SiO2 Am Miner 103:792-802 doi:10.2138/am-2018-6267

Geballe ZM, Jeanloz R (2012) Origin of temperature plateaus in laser-heated diamond anvil cell experiments Journal of Applied Physics 111:123518

Inamura Y, Katayama Y, Utsumi W, Funakoshi K (2004) Transformations in the intermediate-range structure of SiO_2 glass under high pressure and temperature Phys Rev Lett 93

Lin JF et al. (2007) Electronic bonding transition in compressed SiO_2 glass Phys Rev B 75

Luo SN, Cagin T, Strachan A, Goddard WA, Ahrens TJ (2002) Molecular dynamics modeling of stishovite Earth Planet Sci Lett 202:147-157

Meade C, Hemley RJ, Mao HK (1992) High-pressure X-ray diffraction of SiO_2 glass Phys Rev Lett 69:1387-1390

Murakami M, Bass JD (2010) Spectroscopic Evidence for Ultrahigh-Pressure Polymorphism in SiO_2 Glass Phys Rev Lett 104

Petitgirard S et al. (2017) SiO_2 Glass Density to Lower-Mantle Pressures Phys Rev Lett 119

Prescher C, Prakapenka VB (2015) DIOPTAS: a program for reduction of two-dimensional X-ray diffraction data and data exploration High Pressure Research 35:223-230

Prescher C, Prakapenka VB, Stefanski J, Jahn S, Skinner LB, Wang YB (2017) Beyond sixfold coordinated Si in SiO_2 glass at ultrahigh pressures Proc Natl Acad Sci U S A 114:10041-10046

San LT, Hong NV, Hung PK (2016) Polyamorphism of liquid silica under compression based on five order-parameters and two-state model: a completed and unified description High Pressure Research 36:187-197

Sanloup C et al. (2013) Structural change in molten basalt at deep mantle conditions Nature 503:104-+
Sato T, Funamori N (2010) High-pressure structural transformation of SiO2 glass up to 100 GPa Phys Rev B 82
Schultz E et al. (2005) Double-sided laser heating system for in situ high pressure-high temperature monochromatic x-ray diffraction at the ESRF High Pressure Research 25:71-83
Shen G, Lazor P (1995) Measurement of melting temperatures of some minerals under lower mantle conditions J Geophys Res 100:17699-17713
Stixrude L, Karki BB (2005) Structure and freezing of $MgSiO_3$ liquid in the Earth's lower mantle Science 310:297-299
Takada A, Bell RG, Catlow CRA (2016) Molecular dynamics study of liquid silica under high pressure Journal of Non-Crystalline Solids 451:124-130
Usui Y, Tsuchiya T (2010) Ab Initio Two-Phase Molecular Dynamics on the Melting Curve of SiO_2 J Earth Sci 21:801-810
Wang FL, Tange Y, Irifune T, Funakoshi K (2012) P-V-T equation of state of stishovite up to mid-lower mantle conditions J Geophys Res: Solid Earth 117:B06209
Weck G, Garbarino G, Ninet S, Spaulding D, Datchi F, Loubeyre P, Mezouar M (2013) Use of a multichannel collimator for structural investigation of low-Z dense liquids in a diamond anvil cell: Validation on fluid H_2 up to 5 GPa Rev Sci Instr 84
Wu M, Liang Y, Jiang J-Z, Tse JS (2012) Structure and Properties of Dense Silica Glass Scientific Reports 2
Zhang JZ, Liebermann RC, Gasparik T, Herzberg CT, Fei YW (1993) Melting and subsolidus relations of SiO_2 at 9-14 GPa J Geophys Res: Solid Earth 98:19785-19793

FIGURES AND TABLES

Figure 1: Typical temperature measurements. Thermal emission spectra were recorded at the center of the laser spot for sample temperatures of e.g. 5010 K (left) and 6140 K (right), using the online optical system installed at the ID27 beamline. The raw spectra (upper frames) are corrected by the response of the optical system (itself calibrated with a W-lamp at 2600 K) and fitted using the Wien law (middle frames). The so-called "two-color" methods (lower frames) shows a temperature variation of less than 10% of the mean temperature within a range of wavelength from ~670 to ~870 nm, which establishes the good quality of the thermal emission spectra. Temperature measurements are performed with a precision of ±100 K and a reproducibility better than ±30 K.

Figure 2A: **X-ray evidences for melting of SiO_2 at ~40 GPa**. Time elapses from bottom to top. Temperature uncertainty is +/- 100 K. After crystallization of stishovite, continuous rings remain clearly visible up to more than 5000 K. At 5100 K the intensity of SiO_2 diffraction lines is already significantly decreased. At sample temperatures of 5600 and 5400 K, the only remaining diffraction lines come from the KCl pressure medium. Diffraction lines of stishovite reappear when the laser power is decreased to 5050 K, evidencing the SiO_2 recrystallization.

Figure 2B: X-ray evidence for the melting of SiO_2 at 105 GPa. Time elapses from top to bottom. For temperatures lower than 6200 K, the set of diffraction lines evidences the presence of the $CaCl_2$-form of SiO_2 (see Fig. 4) in addition to the KCl pressure medium. The intensity of the SiO_2 peaks decreases severely at 6300-6400 K before they almost disappear at 6500 K. The stishovite to KCl ratio of diffraction peaks intensity decreases by a factor of 10 around between 6200 and 6500 K.

Figure 3: **Melting curve of SiO_2 up to ~120 GPa**. We report temperatures of solid (blue) and liquid (red) SiO_2 together with a smooth trend through the data set (grey band). Our temperature and pressure uncertainties are 200 K and 5 GPa, respectively. We also plot previous melting curve determinations based on early experimental works (Shen and Lazor 1995; Zhang et al. 1993) (light blue), theoretical calculations (purple (Usui and Tsuchiya 2010), blue (Belonoshko and Dubrovinsky 1995) and green (Luo et al. 2002)) and shock wave

experiments (orange (Akins and Ahrens 2002)). For the latter, we report Hugoniot plots in solid and molten states for starting materials composed of quartz and fused-quartz.

Figure 4: Subsolidus transition from Stishovite to the $CaCl_2$-form between 75 and 102 GPa: The stishovite model fits well the upper diffraction pattern recorded at ~75 GPa and ~4500 K. In contrast, the diffraction pattern recorded at ~102 GPa and ~5400 K is not well fitted with the stishovite model (middle frame), but instead with the $CaCl_2$-form model (lower pattern). At these conditions, the $CaCl_2$-form presents (a, b, c) unit cell parameters of (3.831(6), 3.967(5), 2.543(3)). Black, red and blue profiles are experimental data, background and Rietveld fit, respectively.

Figure 5: Structure factor of the compressed glass: As previously noticed (e.g. (Prescher et al. 2017) and references therein), a new contribution around 3-3.5 $Å^{-1}$ grows above ~20 GPa.

Figure 6: Structure factors S(Q) of SiO_2 recorded in the melt between ~38 and ~76 GPa. Spectra recorded at high temperature in the melt at pressures of 38 GPa (orange), 40 GPa (bleu), 54 GPa (grey) and 76 GPa (yellow) are bracketed between spectra recorded at 300 K in the glass compressed to ~18.5 GPa (green) and ~49.5 GPa (dark blue). The contributions observed for the melt below and above ~45 GPa are comparable to those of the glass at ~18.5 GPa and ~49.5 GPa, respectively. It indicates an evolution of the SiO_2 melt structure between 40 and 54 GPa comparable to that reported during the compression of the glass (Fig. 5).

Figure 7: Diffuse scattering signals of melt and quenched glass. The quenched glass (orange, recorded at 8 GPa and 300 K) presents a FSDP position significantly sharper and at slightly higher Q position compared to the corresponding melt (blue, recorded at 26 GPa and ~5150 K). This suggests less densification of the local structure of SiO_2 melt at high temperature, compared to the glass. We did not successfully produced a glass at experimental pressures exceeding 45 GPa, because of full sample crystallization.

Figure 8: Pressure dependence of the first sharp diffraction peak. Our measurements performed in melts (Red) and in glasses either quenched from high temperature (Blue) or during cold-compression (Green) are compared with previous reports. The shift of the FSDP to high wavenumbers occurs at lower pressures in the glass, compared to the melt.

Table 1. Melting temperatures: Sample temperatures are directly provided by radio-spectrometry (Fig. 1). Sample pressures are derived from cross correlation between two methods: the P-V-T equation of state of stishovite and an empirical model of thermal pressure (see text). Experimental uncertainties are within 5 GPa and 100 K.

Table 2. Clapeyron relations: Volumes and entropies relations calculated around (i) the true triple point where coesite, stishovite and LDM coexist and (ii) the fictive triple point where LDM, HDM and stishovite would coexist (see text). Thermodynamical parameters come from (Akaogi et al. 2011; Wang et al. 2012; Zhang et al. 1993).

Fig. 1

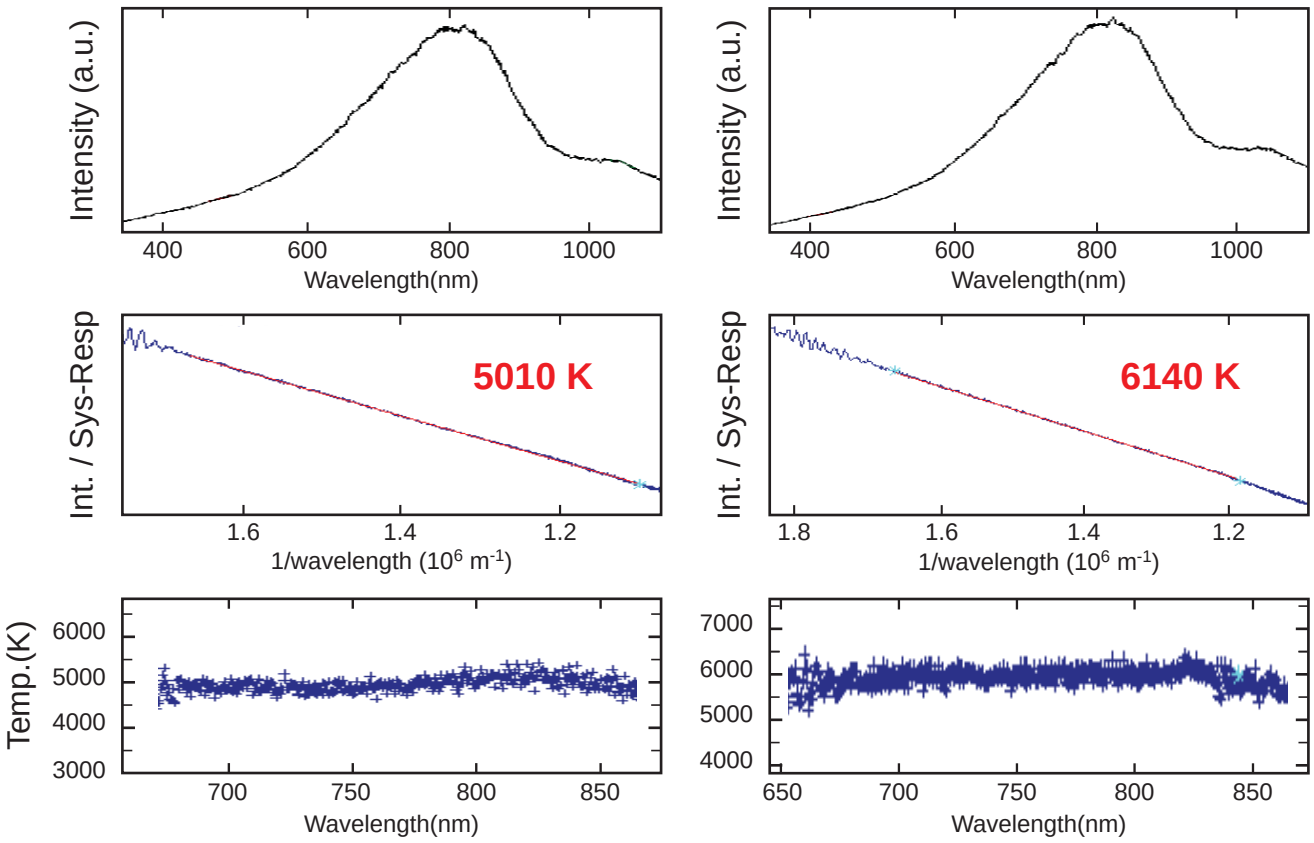
Intensity (a.u.)
400
600
800
1000
Wavelength(nm)
Int. / Sys-Resp
5010 K
1.6
1.4
1.2
1/wavelength (10^6 m^-1)
Temp.(K)
6000
5000
4000
3000
700
750
800
850
Wavelength(nm)
Intensity (a.u.)
400
600
800
1000
Wavelength(nm)
Int. / Sys-Resp
6140 K
1.8
1.6
1.4
1.2
1/wavelength (10^6 m^-1)
7000
6000
5000
4000
650
700
750
800
850
Wavelength(nm)

Fig. 2A

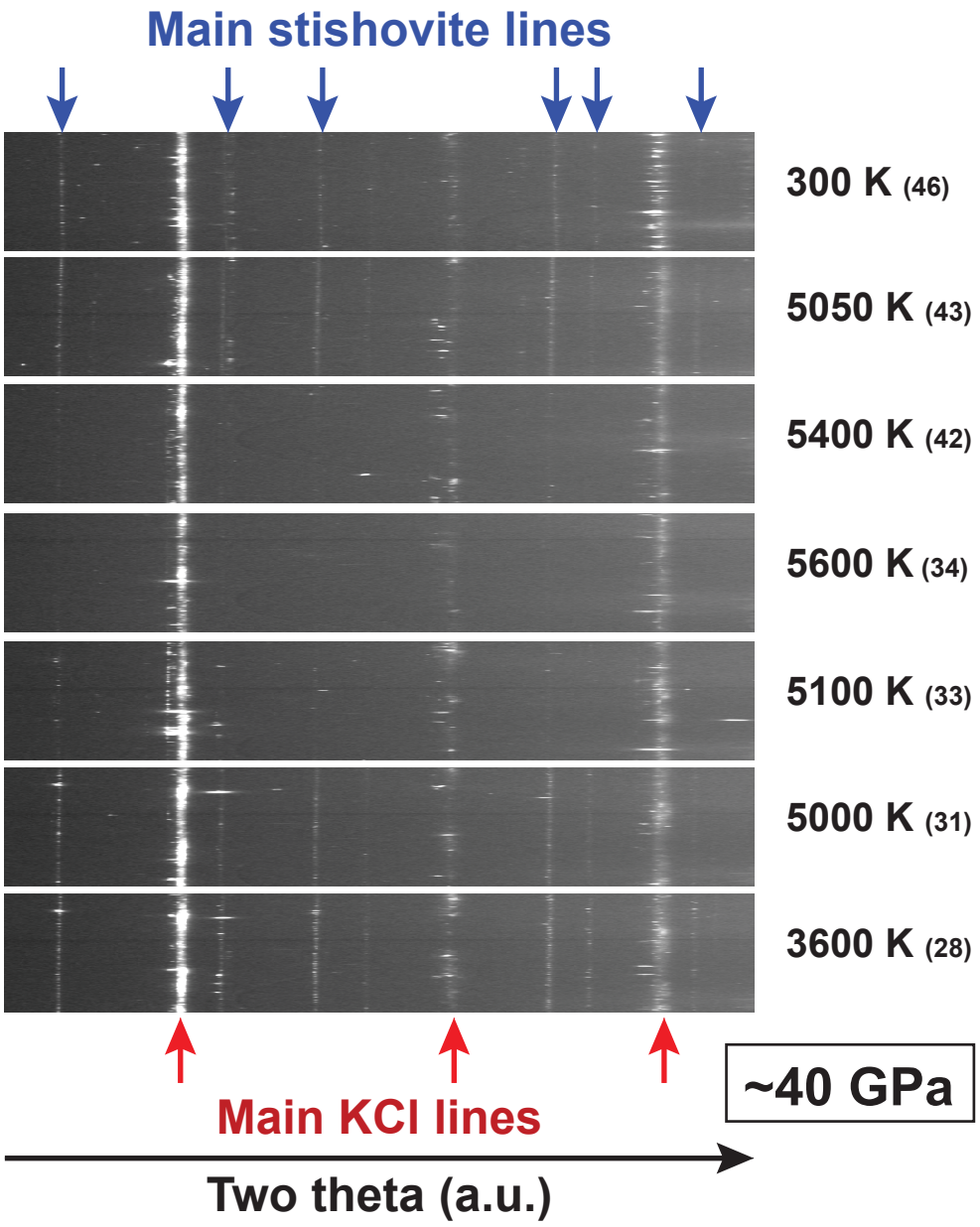
Main stishovite lines
300 K (46)
5050 K (43)
5400 K (42)
5600 K (34)
5100 K (33)
5000 K (31)
3600 K (28)
Main KCl lines
~40 GPa
Two theta (a.u.)

Fig. 2B

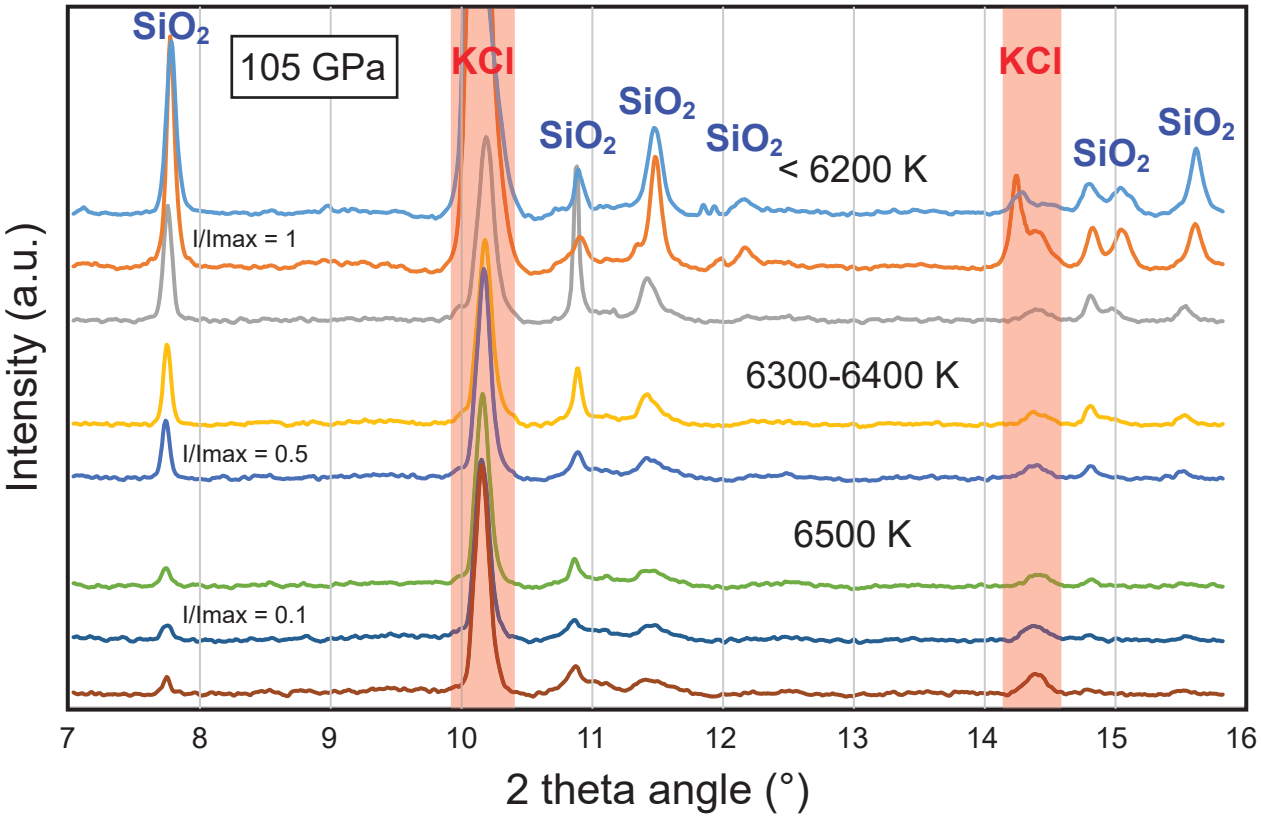
SiO2
105 GPa
KCl
SiO2
SiO2
SiO2
< 6200 K
KCl
SiO2
SiO2
I/Imax = 1
6300-6400 K
I/Imax = 0.5
6500 K
I/Imax = 0.1
Intensity (a.u.)
7
8
9
10
11
12
13
14
15
16
2 theta angle (°)

Fig. 3

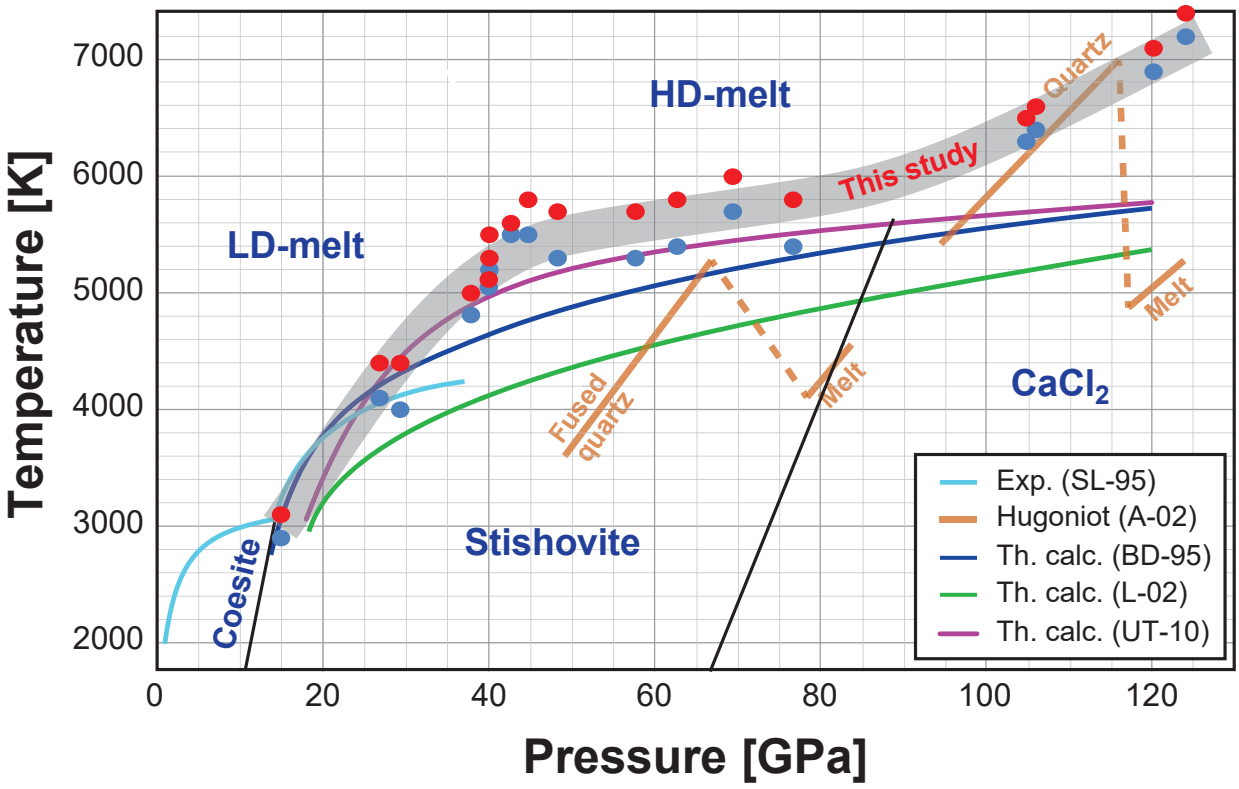
Temperature [K]
7000
6000
5000
4000
3000
2000
0
20
40
60
80
100
120
Pressure [GPa]
HD-melt
LD-melt
Stishovite
Coesite
This study
Quartz
Melt
Fused quartz
Melt
CaCl2
Exp. (SL-95)
Hugoniot (A-02)
Th. calc. (BD-95)
Th. calc. (L-02)
Th. calc. (UT-10)

Fig. 4

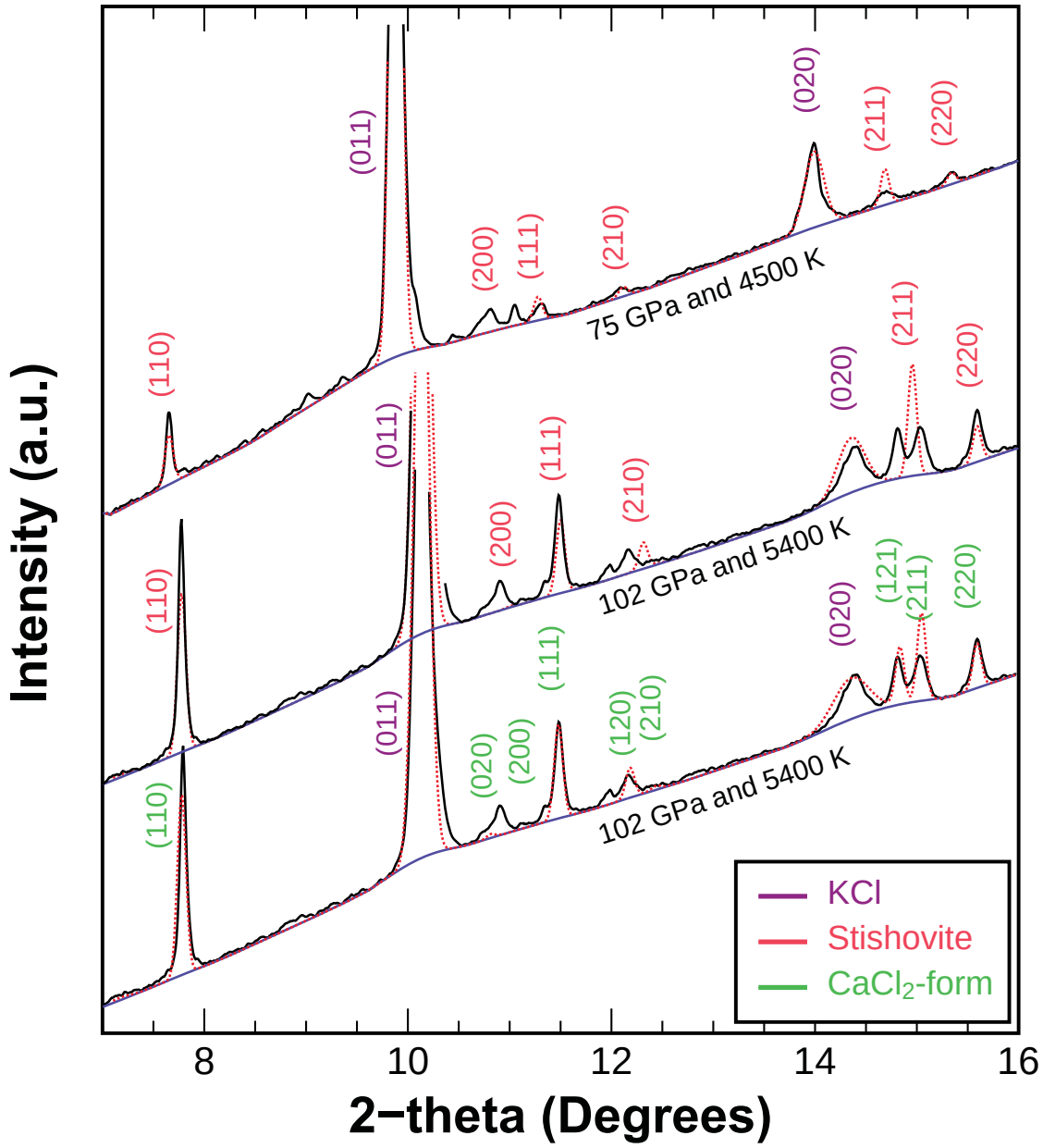
Intensity (a.u.)
2−theta (Degrees)
8
10
12
14
16
(011)
(020)
(211)
(220)
(200)
(111)
(210)
(110)
75 GPa and 4500 K
102 GPa and 5400 K
102 GPa and 5400 K
(121)
(120)
KCl
Stishovite
CaCl2-form

Fig. 5

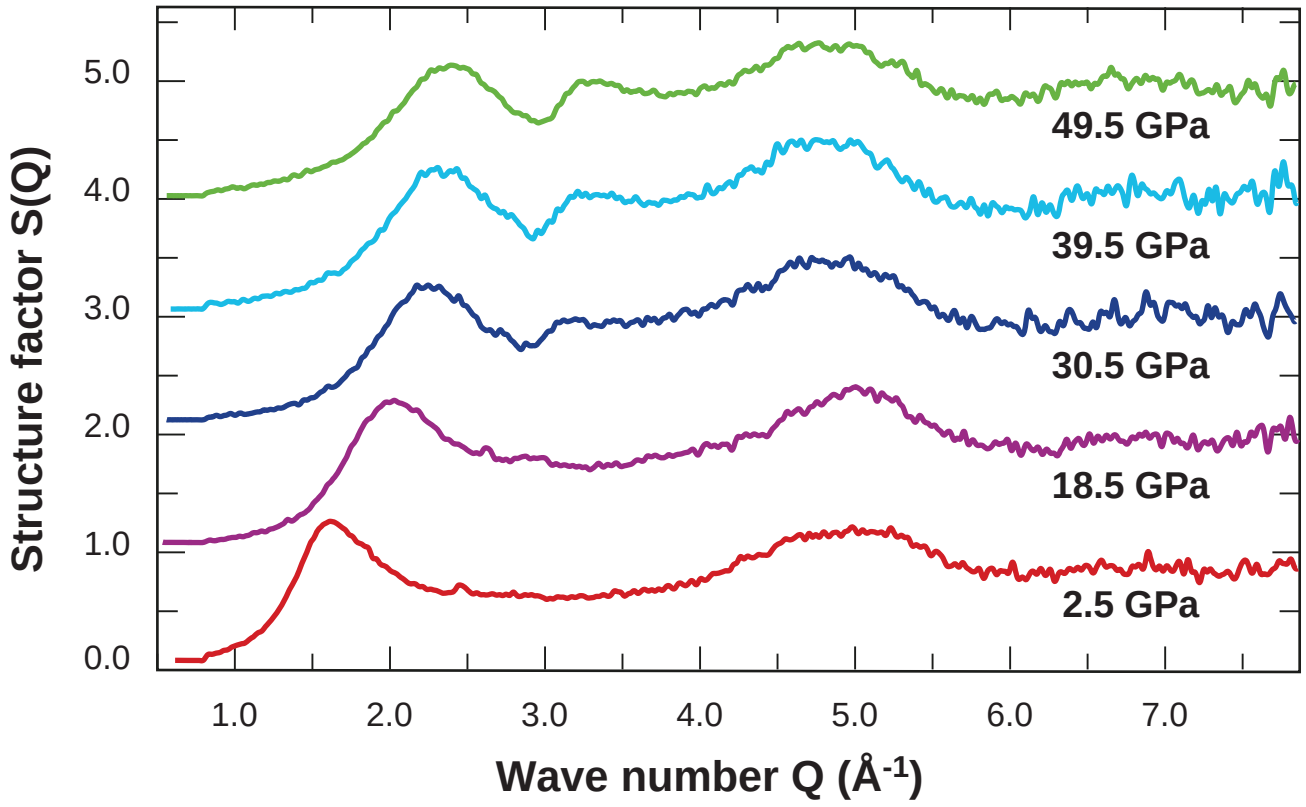
Structure factor S(Q)
5.0
4.0
3.0
2.0
1.0
0.0
49.5 GPa
39.5 GPa
30.5 GPa
18.5 GPa
2.5 GPa
1.0
2.0
3.0
4.0
5.0
6.0
7.0
Wave number Q (Å-1)

Fig. 6

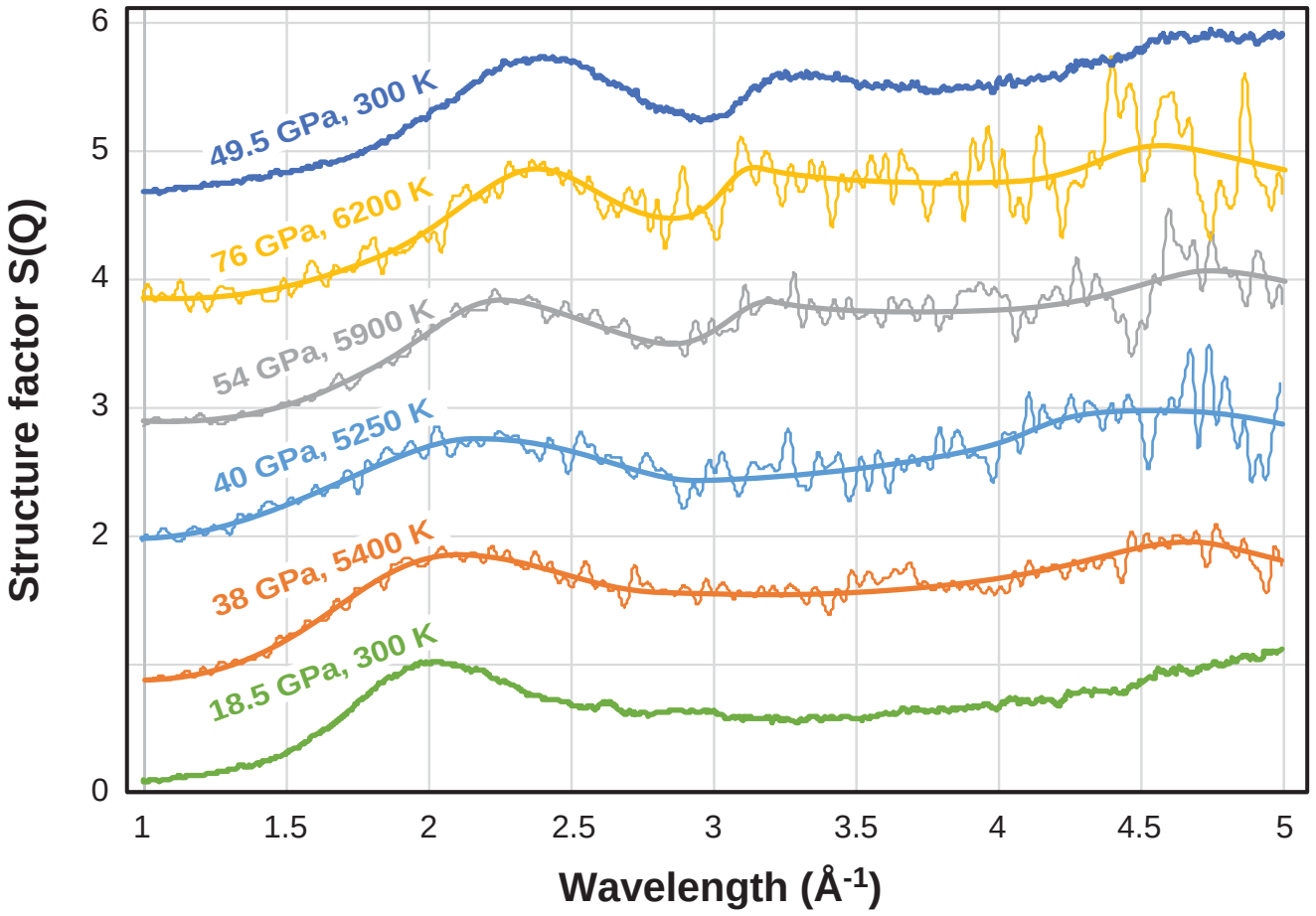
Structure factor S(Q)
Wavelength (Å-1)
49.5 GPa, 300 K
76 GPa, 6200 K
54 GPa, 5900 K
40 GPa, 5250 K
38 GPa, 5400 K
18.5 GPa, 300 K
0
2
3
4
5
6
1
1.5
2
2.5
3
3.5
4
4.5
5

Fig. 7

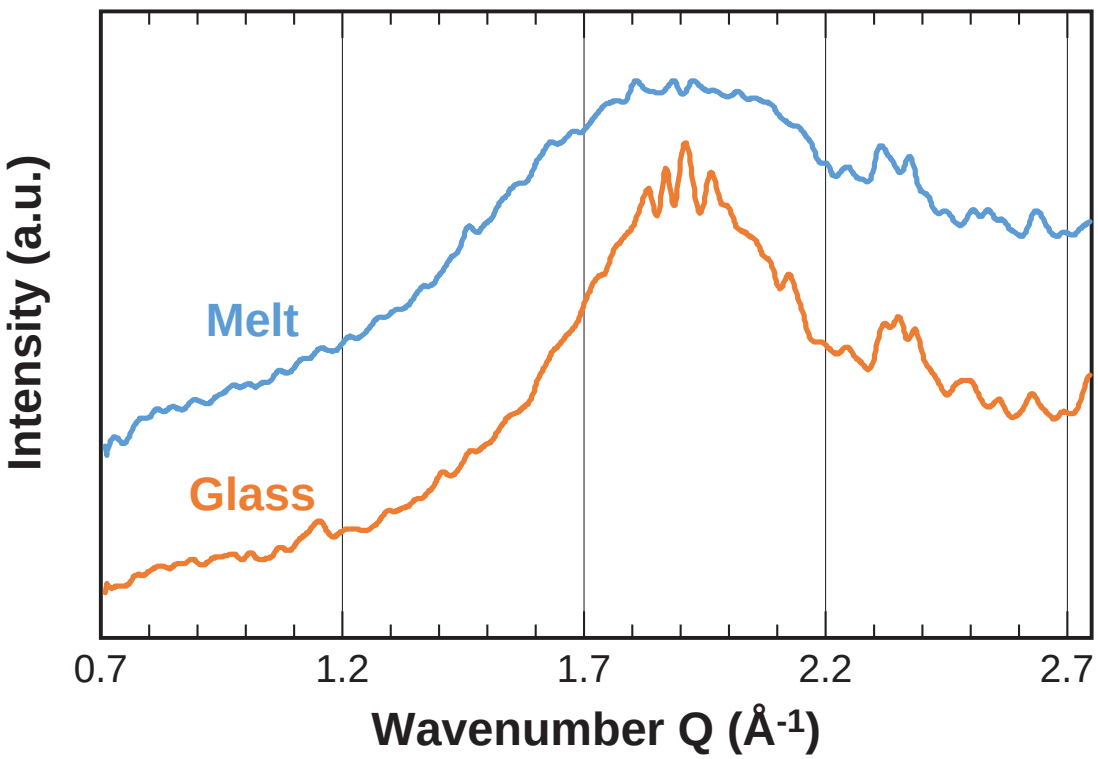

Fig. 8

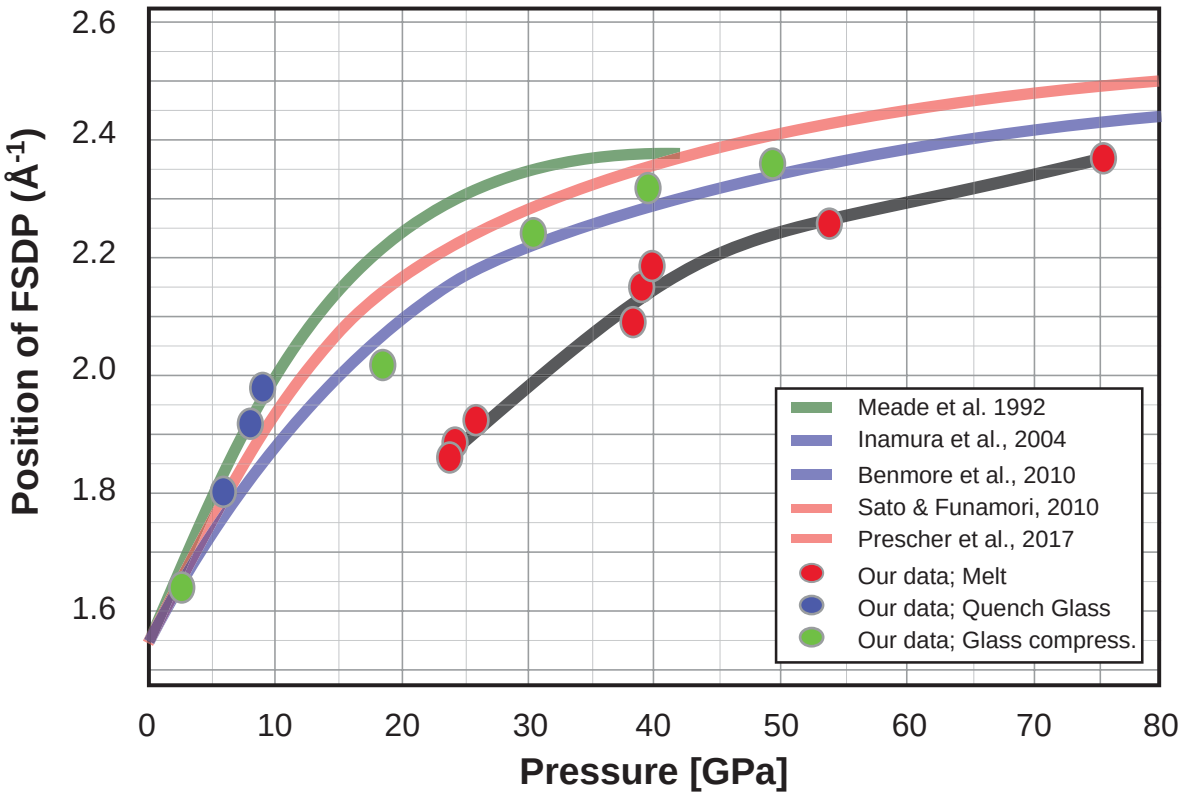
Position of FSDP (Å-1)
2.6
2.4
2.2
2.0
1.8
1.6
0
10
20
30
40
50
60
70
80
Pressure [GPa]
Meade et al. 1992
Inamura et al., 2004
Benmore et al., 2010
Sato & Funamori, 2010
Prescher et al., 2017
Our data; Melt
Our data; Quench Glass
Our data; Glass compress.

Table-2

Transition considered	Press. GPa	Temp. K	dT/dP K/GPa	DS mol/K	DV cm3/mol	Vstish cm3/mol	Vcoes cm3/mol	VLDM cm3/mol	VHDM cm3/mol	DV/V
C => S	15	3023	312 a	-15.28 a	-4.76736 b	14.6916 g	19.459 h			-0.279 k
C => LDM	15	3023		74.9 d	0 e		19.459 h			
S => LDM	15	3023	80 *	59.59 b	4.76736 g	14.6916 g		19.459 i		0.2792 k
S => HDM	45	5400	12.5 *	74.59 d	0.9324 b	13.6434 g			14.5758 j	0.0661 k
LDM=>HDM	45	5400		-15 c	-3.83496 f			18.4108 i	14.5758 j	-0.233 k
S => HDM	45	5400	12.5 *	59.59 d	0.7449 b	13.6434 g			14.3883 j	0.0531 k
LDM=>HDM	45	5400		0 c	-4.02246 f			18.4108 i	14.3883 j	-0.245 k
S => HDM	45	5400	12.5 *	44.59 d	0.5574 b	13.6434 g			14.2008 j	0.04 k
LDM=>HDM	45	5400		15 c	-4.20996 f			18.4108 i	14.2008 j	-0.258 k

C, S, LDM and HDM stand for Coesite, Stishovite, low-density and high-density SiO2 melts
*, this study
a, from Akaogi et al. (2011)
b, calculated based on the Clapeyron relation dT/dP=DV/DS
c, value assumed to be -15, 0 or 15 J/molK (see text)
d, derived from Clapeyron relations around the (C, S, LDM) or (C, LDM, HDM) triple points
e, derived from the flat melting curve of coesite between 9 and 14 GPa (Zhang et al., 1993)
f, calculated using DV=VHDM-VLDM
g, calculated at the considered P-T conditions using the EoS of Wang et al. (2012)
h, calculated using Vcoes=Vsti+DV(C-S)
i, calculated using VLDM=Vsti+DV(LDM-S)
j, calculated using VHDM=Vsti+DV(HDM-S)
k, DV of the transition normalized to the mean value between the two phases considered

Table-1

P(300K) GPa	Temp. K	P(high-T) GPa	Temp solid	Temp Melt
12	3000	15	2900	3100
16	4250	27	4100	4400
19	4200	29	4000	4400
19	5350	40	5200	5500
19.5	5100	40	5050	5100
20	5500	43	5500	5600
21	5600	45	5500	5800
21.5	4900	38	4800	5000
21.5	5100	40	5000	5300
26	5500	48	5300	5700
36	5500	58	5300	5700
39	5700	63	5400	5800
45	5800	69	5700	6000
54	5700	77	5400	5800
76	6500	106	6400	6600
76	6400	105	6300	6500
85	7300	124	7200	7400
85	7000	120	6900	7100